Proceedings of the European Conference Physics of Magnetism, Poznań 2014

Kondo-Fano Effect in Double Quantum Dot Side Attached to a Pair of Wires

D. Krychowski* and S. Lipiński

Institute of Molecular Physics, Polish Academy of Sciences, M. Smoluchowskiego 17, 60-179 Poznań, Poland

Electron tunneling through a double quantum dot side coupled to a pair of leads is examined in finite-U slave boson mean field approach. Both the two-impurity Kondo regime at half filling and one-and three-electron Kondo effects are analyzed. Special attention is paid to the case when one of the dots is coupled to ferromagnetic lead and another to nonmagnetic. Depending on the gate voltage, the same or opposite sign of polarizations of conductance of the leads is observed.

DOI: 10.12693/APhysPolA.127.487

PACS: 72.10.Fk, 73.21.–b, 73.22.–f, 73.23.–b

1. Introduction

Recently double dot systems (DQD) have been investigated due to their potential applicability as single electron transistors or as building blocks of quantum computers (coupled qubits) [1]. Owing to the tunability of couplings especially rich physics emerges in multiply connected geometries due to the interplay of strong correlations and interference [2–8]. In this paper we study two tunnel-coupled interacting quantum dots (DQD) side-coupled to a pair of quantum wires (TDQD) (inset of Fig. 1b). We focus on the Kondo range, discussing both atomic and molecular Kondo regimes. In the former case we analyze the role of singularities of density of states (DOS) of the leads on Kondo-Fano physics and compare the results for rectangular density of states with DOS characterized by Van Hove singularities (VHS). As the illustrative examples of singular DOS we choose carbon nanotube and graphene nanoribbon. Coupling of DQD to magnetic electrodes is another objective of this paper. We show how TDQD can be used in transferring polarization of conductance.

2. Model

We consider two neighboring quantum dots or adatom dimer coupled to a pair of leads. The corresponding Hamiltonian reads:

$$\mathcal{H} = t' \sum_{\alpha i \sigma} (c^{\dagger}_{i\alpha\sigma} c_{i+1\alpha\sigma} + h.c.) + \varepsilon_0 \sum_{\alpha\sigma} c^{\dagger}_{0\alpha\sigma} c_{0\alpha\sigma} + \varepsilon_d \sum_{\alpha\sigma} f^{\dagger}_{\alpha\sigma} f_{\alpha\sigma} + \mathcal{U} \sum_{\alpha} n_{\alpha\uparrow} n_{\alpha\downarrow} + t \sum_{\sigma} (f^{\dagger}_{1\sigma} f_{2\sigma} + h.c.) + \mathcal{V} \sum_{\alpha\sigma} (f^{\dagger}_{\alpha\sigma} c_{0\alpha\sigma} + \text{H.c.}) \quad (1)$$

The first term describes electrons in the electrodes ($\alpha = 1, 2$), the second represents gate voltage ε_0 applied to these sites of the wires, which are tunnel-coupled to the dots ("interface sites" labeled as 0α). The third and fourth terms describe interacting dots specified by site energy ε_d and Hubbard repulsion $\mathcal{U}$, and the last two terms account for interdot tunneling t and tunneling to the leads $\mathcal{V}$. Gate voltage allows for the control of interference conditions. For the rectangular density of states of electrodes Fano parameter specifying transmission line shape is given by $q = \frac{\varepsilon_0}{\Gamma}$ with $\Gamma = \frac{\pi t'^2}{2\mathcal{D}}$, and $\mathcal{D}$ is the electrodes half bandwidth. In the finite-U slave boson approach [9], a set of auxiliary bosons e_α, $p_{\alpha\sigma}$, d_α are introduced for each dot, which act as projection operators onto empty, simply occupied (with spin up or spin down), and doubly occupied electron states on quantum dot, respectively. The full Hilbert space has to be restricted to physically meaningful sector by imposing constraints i.e. completeness relations $e^{\dagger}_{\alpha} e_\alpha + \sum_{\alpha\sigma} p^{\dagger}_{\alpha\sigma} p_{\alpha\sigma} + d^{\dagger}_{\alpha} d_\alpha = 1$ and charge conservations $\mathcal{Q}_{\alpha\sigma} = f^{\dagger}_{\alpha\sigma} f_{\alpha\sigma} = p^{\dagger}_{\alpha\sigma} p_{\alpha\sigma} + d^{\dagger}_{\alpha} d_\alpha$. These constraints are incorporated into the Hamiltonian with Lagrange multipliers λ, $\lambda_{\alpha\sigma}$. In the mean field approximation (SBMFA) the slave boson operators are replaced by their expectation values and the problem is formally reduced to the free-particle model with renormalized hopping integrals $\widetilde{\mathcal{V}} = \mathcal{V} z_{\alpha\sigma}$, $\widetilde{t} = t z^{\dagger}_{1\sigma} z_{2\sigma}$ with $|z_{\alpha\sigma}| = \frac{e^{\dagger}_{\alpha} p_{\alpha\sigma} + p^{\dagger}_{\alpha\bar{\sigma}} d_\alpha}{\sqrt{\mathcal{Q}_{\alpha\sigma}} \sqrt{1 - \mathcal{Q}_{\alpha\sigma}}}$ and renormalized site energies $\widetilde{\varepsilon}_{\alpha\sigma} = \varepsilon_d + \lambda_{\alpha\sigma}$. The stable solutions are then found from the minimum of the free energy with respect to the mean values of boson operators and Lagrange multipliers. The current flowing through the wires is calculated from the time evolution of occupation numbers of "interface sites", and is given by $\mathcal{I}_{\alpha\sigma} = \frac{e}{\hbar} t' \sum_k (\mathcal{G}^{<}_{0\alpha\sigma, k\alpha\sigma} - \mathcal{G}^{<}_{k\alpha\sigma, 0\alpha\sigma})$, where $\mathcal{G}^{<}_{0\alpha\sigma, k\alpha\sigma}$ are dot-wire lesser Green's functions. The linear conductance is defined by $g_{\alpha\sigma} = \frac{d\mathcal{I}_{\alpha\sigma}}{dV}|_{V \to 0}$ and polarization of conductance by $\mathrm{PC}(\alpha) = \frac{g_{\alpha\uparrow} - g_{\alpha\downarrow}}{g_{\alpha\uparrow} + g_{\alpha\downarrow}}$.

3. Results and discussion

Figure 1 presents TDQD conductance, occupations and characteristic temperatures specifying strengths of many-body correlations for different interdot tunneling. Fig. 1a shows symmetric ($q = 0$) conductance with particle-hole $\varepsilon_d = \frac{-\mathcal{U}}{2}$ symmetry line. For $t = 0$ the

*corresponding author; e-mail: krychowski@ifmpan.poznan.pl

single dot Kondo effects occurring near half filling provide a suppression of the transmissions of the wires due to destructive interference of the ballistic channels and Kondo channels.

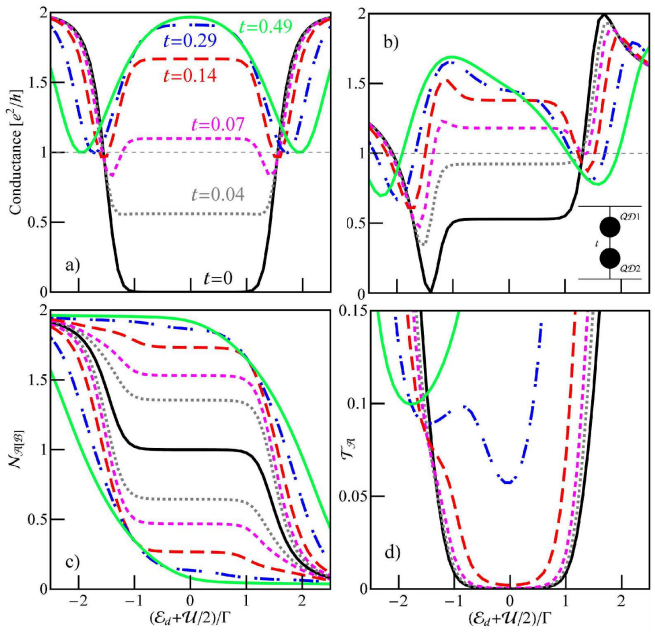

Fig. 1. Linear conductance at the "interface" (0α) site of the wire as a function of the dot level for various values of interdot coupling (a) $q = 0$, (b) $q = 0.6$. Inset shows schematic plot of TDQD system. (c) Occupations of bonding and antibonding orbitals (d) Characteristic temperature specifying position and width of many body resonance of electrons in antibonding orbital. $\mathcal{T}_A$ plays the role of Kondo temperature for strong interdot coupling in the range of almost completely filled bonding orbital and single occupied antibonding orbital. In the weak interdot coupling limit $\mathcal{T}_A$ can serve as Kondo temperature in the range of half occupancy. Parameters used are $\mathcal{U}/\Gamma = 3$ and $\mathcal{V}/\Gamma = 0.25$.

On the other limit of empty dots or full occupancy the couplings between the dots and the wires become ineffective and the conductance approaches conductance quantum due to the ballistic transmission through the wires. Increase of interdot coupling splits the Kondo resonances forming the dips of wire transmissions on both sides of the Fermi energy what results in an increase of conductance around half filling. For large values of interdot couplings ($t > \mathcal{V}$) it is more natural to consider the attached subsystem as a molecule connected to the wires with bonding (B) and antibonding (A) orbitals (compare the increasing differenence of occupations of these two orbitals presented in Fig. 1c). Around half filling the bonding orbital is almost fully occupied and antibonding empty. Kondo effect does not occur in this case and transport channel through the molecule becomes more and more inefficient with the increase of t, what results in recovery of high transparency of the wires. Close to the one or three electron occupancies, however, for large interdot couplings the additional conductance minima emerge, which are the manifestations of single electron or single hole Kondo effects. For $N = 1$ the role of Kondo active orbital play bonding and for $N = 3$ antibonding orbital, the complementary orbital is then empty or completely filled (Fig. 1c).

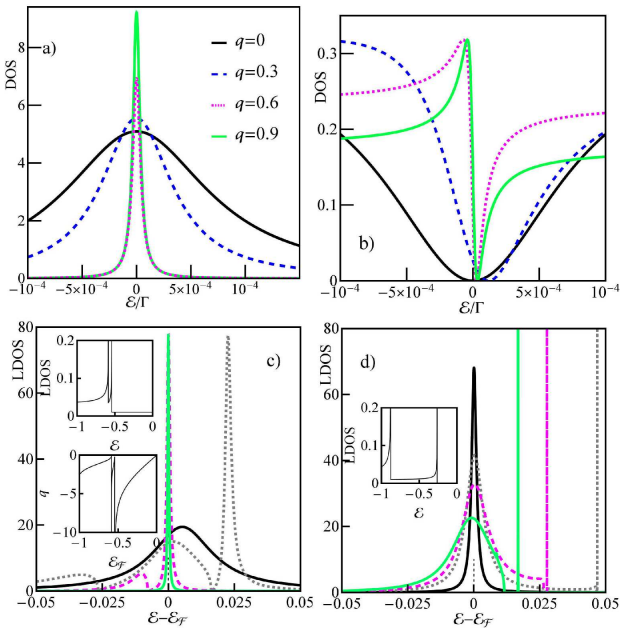

Fig. 2. (a) Comparison of densities of states of T-shaped system (TDQD for $t = 0$) with electrodes characterized by rectangular density of states ((a) and (b)) and with singular electrodes (c) metallic - zigzag CNT(24,0) and semiconducting graphene nanoribbon 12-AGNR. The LDOS curves in Figures c,d are plotted for different values of chemical potential: black solid line $\varepsilon_F = -0.79$ (c), $\varepsilon_F = -0.5$ (d), dotted line $\varepsilon_F = -0.56$ (c), $\varepsilon_F = -0.3$ (d), dashed line $\varepsilon_F = -0.536$ (c), $\varepsilon_F = -0.289$ (d) and gray/green solid line $\varepsilon_F = 0$ (c), $\varepsilon_F = -0.274$ (d). Insets show carbon nanotube DOS and AGNR DOS and Fano asymmetry parameter. Parameters used are $\mathcal{U}/\Gamma = 3$ and $\mathcal{V}/\Gamma = 0.25$ for TQD and $\mathcal{U} = 3$ eV , $V = 0.7$ eV and $t' = 2.5$ eV for impurities attached to CNT and AGNR.

The characteristic temperatures defined by positions ($\widetilde{\varepsilon_\nu}$, $\nu = A, B$) and the widths ($\widetilde{\Delta_\nu}$) of corresponding many-body peaks ($\mathcal{T}_\nu = \sqrt{\widetilde{\varepsilon_\nu}^2 + \widetilde{\Delta_\nu}^2}$) determine Kondo temperatures in the range near single occupancy of Kondo active orbitals ($\mathcal{T}_A(\mathcal{E}) = \mathcal{T}_B(-\mathcal{E})$) (Fig. 1d). Note that due to the weaker coupling determined mainly by direct coupling to the leads, atomic Kondo temperatures ($N = 2$) are much lower than molecular Kondo temperatures ($N = 1, 3$). Fig. 1b presents asymmetric conductances characterized by minimum and maximum on the opposite sides of $\varepsilon_d = \frac{-\mathcal{U}}{2}$ line for the weak interdot coupling and by two minima and maximum for the strong coupling. Fully destructive and constructive interference manifesting in entering of the zero transmission dip or unitary maximum on the Fermi level is only

observed in the limit of $t = 0$. For coupled dots ($t \neq 0$), a suppression or enhancement of conductance is not complete, due to the additional interdot interference channel. In the range of single electron or single hole Kondo effects again interference processes lead to suppression of conductance with minima located asymmetrically with respect to electron-hole symmetry line and correspondingly with different values of conductivity. So far we have considered the case, where interference conditions change monotonically with the gate voltage. Representative local densities of states (LDOS) at interacting dots and at the "interface sites" of the wires are presented on Fig. 2a and b, for brevity shown only for $t = 0$ case. Increase of Fano parameter only slightly perturbs symmetry of Kondo resonances of interacting dots, but considerably narrows the Kondo lines. For electrodes with divergent singularities in the densities of states and consequently singular hybridization, e.g. for carbon nanotubes or graphene nanoribbons dramatic changes of both Kondo physics and interference conditions are expected when Fermi levels enters VHS.

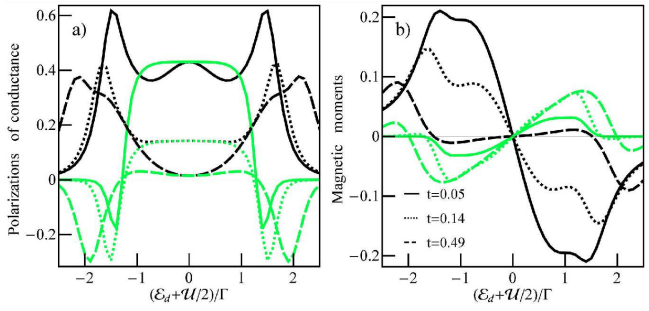

Fig. 3. Polarization of conductances (a) and magnetic moments (b) at the dots of TDQD with upper ferromagnetic electrode and lower paramagnetic presented for various values of interdot coupling. Black curves represent upper electrode and upper dot ($\alpha = 1$) and grey/green curves lower ($\alpha = 2$). Polarization of ferromagnetic electrode P= 0.6 and the rest of parameters as in Fig. 1.

The evolution of densities of states with the shift of the Fermi level for single impurity side attached to metallic single wall carbon nanotube (SWCNT) and to semiconducting graphene nanoribbon (AGNR) are presented (Fig 2c and d). The effective Fano parameter $q = \mathcal{R}e[\mathcal{G}^R_{0\alpha\sigma}]/\mathcal{I}m[\mathcal{G}^R_{0\alpha\sigma}]$ exhibits discontinuous changes around VHS (inset of Fig. 2c). In the range of constant density of states far away from VHS (range of linear dependence of q with energy), the resonance peak at impurity is symmetric (Fig. 2c), similarly to the previously discussed cases. Closer to VHS, singularities manifest as the dips in DOS, the central peak splits, broadens and gets strongly asymmetric. All these anomalies are the consequence of enhanced imaginary part of hybridization and a jump from positive to negative values of the real part of hybridization. In close proximity to singularities, however, the presented results should be treated with caution only as visualization of tendencies, due to a break of applicability of SBMFA in the range of divergent self-energy [10]. For system with the gap (AGNR) delta-like structures are observed at the band edges, which extend into the gap for ε_F moving very close to the edge. They reflect the new poles of the impurity Green's function lying on the real axis, and these structures are essential in order to satisfy the sum rules. Wide tunability of DQDs build into an electric circuit with magnetic electrodes can be also exploited in spintronics. Figure 3a shows the example of transfer of spin polarization of conductance between ferromagnetic and paramagnetic wires. Depending on the gate voltage the induced spin polarization of conductance (PC) of the paramagnetic lead can be of the same sign as PC of ferromagnetic lead (single dot Kondo regime) or opposite (molecular Kondo regime). Fig. 3b signals also the possibility of gate control of orientations of magnetic moments of the dots, but to get a deeper insight into this problem within slave boson formalism it is indispensable to introduce an extra antiferromagnetic interdot exchange interaction in the model [11].

Acknowledgments

This project was supported by the Polish National Science Center from funds awarded through the decision No. DEC-2013/10/M/ST3/00488.

References

[1] D. Loss, D.P. DiVinzenzo, *Phys. Rev. A* **57**, 120 (1998).

[2] M. Sato, H. Aikawa, K. Kobayashi, S. Katsumoto, Y. Iye, *Phys. Rev. Lett.* **95**, 066801 (2005).

[3] S. Katsumoto, H. Aikawa, M. Eto, Y. Iye, *Phys. Stat. Sol. (c)* **3**, 4208 (2006).

[4] B. Babić, C. Schönenberger, *Phys. Rev. B* **70**, 195408 (2004).

[5] A. Gruneis, M. J. Esplandiu, D. Garcia-Sanchez, A. Bachtold, *Nano. Lett.* **7**, 3766 (2007).

[6] B.R. Bułka, P. Stefański, *Phys. Rev. Lett.* **86**, 5128 (2001).

[7] S. Lipiński, D. Krychowski, *J. Magn. Magn. Mat.* **310**, 2423 (2007).

[8] P. Trocha, J. Barnaś, *Phys. Rev. B* **76**, 165432 (2007).

[9] G. Kotliar, A. E. Ruckenstein, *Phys. Rev. Lett.* **57**, 1362 (1986).

[10] A.K. Zhuravlev, V.Yu. Irkhin, *Phys. Rev. B* **84**, 245111 (2011).

[11] W. Izumida, O. Sakai, *Phys. Rev. B* **62**, 10260 (2000).